Letter

Meson content of entanglement spectra after integrable and nonintegrable quantum quenches

Johannes Knaute [*]
Racah Institute of Physics, The Hebrew University of Jerusalem, Jerusalem 91904, Givat Ram, Israel

(Received 14 November 2022; revised 4 March 2023; accepted 7 March 2023; published 17 March 2023)

We use tensor network simulations to calculate the time evolution of the lower part of the entanglement spectrum and return rate functions after global quantum quenches in the Ising model. We consider ground state quenches toward mesonic parameter ranges with confined fermion pairs as nonperturbative bound states in a semiclassical regime and the relativistic E_8 theory. We find that in both cases only the dominant eigenvalue of the modular Hamiltonian fully encodes the meson content of the quantum many-body system or quantum field theory, giving rise to nearly identical entanglement oscillations in the entanglement entropy. When the initial state is prepared in the paramagnetic phase, the return rate density exhibits regular cusps at unequally spaced positions, signaling the appearance of dynamical quantum phase transitions, at which the entanglement spectrum remains gapped. Our analyses provide a deeper understanding on the role of quantum information quantities for the dynamics of emergent phenomena reminiscent of systems in high-energy physics.

DOI: 10.1103/PhysRevB.107.L100303

Introduction and motivation. Quantum information concepts became increasingly relevant for the study of entanglement properties in strongly coupled quantum many-body (QMB) systems and quantum field theories (QFTs) in and out of equilibrium [1–3]. While entanglement entropy is the most popular measure to quantify the amount of entanglement in pure states, to extract universal information, or to use it as an order parameter in (quantum) phase transitions (see, e.g., the review [4]), the seminal paper [5] introduced the more general *entanglement spectrum*, which allows one to characterize the entanglement structure of a physical system in a pure state on an even deeper and more complete level.

Consider a pure state density operator ρ and a spatial bipartition into a subsystem A and its complement B. The *modular* (or *entanglement*) *Hamiltonian* $\mathcal{H}_{\mathrm{mod}}$ [6] is then defined from the reduced density matrix ρ_A of the subsystem via

$$\rho_A = \mathrm{Tr}_B \rho \equiv e^{-\mathcal{H}_{\mathrm{mod}}}. \tag{1}$$

The corresponding set of eigenvalues is denoted as the entanglement spectrum, from which the entanglement entropy and Rényi entropies can be calculated. While this concept was originally employed to detect topological order [5,7], it found an enormous amount of attention across different fields in physics (see, e.g., [8] for a review). In particular, it has been studied for lattice models [9–20] and fermionic systems [21–25]. Calculations of $\mathcal{H}_{\mathrm{mod}}$ in QFTs, and especially conformal field theories (CFTs), are based on the Bisognano-Wichmann theorem [26,27], which allowed the authors of [28–31] to find some explicit forms. The modular Hamiltonian and its spectrum have also been studied using tensor networks [32–36] and via holography in connection with further quantum information measures [28,37,38].

In this Letter, we are interested in studying the impact of meson confinement on the dynamics of entanglement spectra after quantum quenches. Mesons are nonperturbative bound states, which appear in quantum chromodynamics (QCD) as flux tube confined quark-antiquark pairs that are important for the physics of the early universe after the big bang and heavy-ion collisions in nuclear accelerators [39–41]. The phenomenology of meson confinement, however, is not exclusive to QCD. Mesonic bound states exist also as confined fermion pairs (domain walls) in the spectrum of the quantum Ising model with longitudinal field [42] or long-range interactions [43,44]. The seminal paper [45] initiated the study of their impact on the entanglement dynamics. Specifically, it was found that mesons give rise to *entanglement oscillations*, i.e., an oscillating behavior of the entanglement entropy after quantum quenches, which bounds the overall entanglement growth if the quench is performed within the ferromagnetic phase and mesons are produced at rest. While analyses of quantum quenches toward critical regimes revealed that the entanglement spectrum carries universal information in the form of the operator scaling dimensions of the underlying boundary CFT [30,46,47], comparable studies in mesonic models have not yet been pursued. We fill this gap in this Letter using tensor network simulations [48,49] for both nonintegrable semiclassical and integrable relativistic regimes of the Ising model at early and intermediate timescales.

We are particularly also interested in differences between quenches within the ferromagnetic phase versus crossings from the paramagnetic one. It hence becomes insightful to discuss our analyses in connection with *dynamical quantum phase transitions* (DQPTs). These are nonequilibrium phase transitions, which occur in the time domain after quenches, showing up as nonanalyticities (cusps) in return rate functions. (For reviews on that topic see [50,51].) Originally discovered through *regular cusps* in [52] for quenches across the critical point of the transverse field Ising model, it was realized

[*]johannes.knaute@mail.huji.ac.il

that DQPTs exist also for phase crossings in the longitudinal field [53] and the long-range Ising model [54,55], i.e., in models where mesons can exist. Their appearance was experimentally confirmed in [56,57]. Moreover, it was shown that *anomalous* DQPTs can even exist for quenches within the ferromagnetic phase [55,58–62]. Connections between DQPTs and the dynamics of the entanglement spectrum have been pioneered in [63–66]. While the necessity of meson states for anomalous DQPTs has been explored in [59,61], their explicit role in the entanglement spectrum has not yet been addressed.

Our analyses are also strongly motivated by significant advances of quantum simulation technologies for the study of fundamental physics problems [67–70]. Recently, the impact of confinement and mesons on quantum correlations, entanglement dynamics, and related properties has been studied experimentally [71,72] and theoretically [73–81]. On the other hand, not only DQPTs became accessible in quantum simulations [56,57], but also the spectrum of the modular Hamiltonian via entanglement tomography [82–84]. It therefore is a very timely problem to address the impact of meson confinement also in the latter context.

Model. The one-dimensional nearest-neighbor quantum Ising model is defined by the Hamiltonian

$$H = -J\left(\sum_{j=1}^{N-1}\sigma_j^z\sigma_{j+1}^z + h\sum_{j=1}^{N}\sigma_j^x + g\sum_{j=1}^{N}\sigma_j^z\right), \qquad (2)$$

where σ_j^α ($\alpha = \{x, z\}$) are Pauli matrices at lattice position j within an open chain of N sites. The unit $J \equiv 1$ sets the overall lattice energy scale, and the transverse and longitudinal field perturbations with respect to the first interaction term are quantified by the parameters h and g, respectively. The transverse model ($g = 0$) exhibits a quantum critical point at $J = h = 1$, at which a quantum phase transition from a disordered paramagnetic phase ($h > 1$) toward an ordered ferromagnetic phase ($h < 1$) occurs [85].

In the thermodynamics limit ($N \to \infty$), there exists a scaling limit, in which the infrared regime is described by a

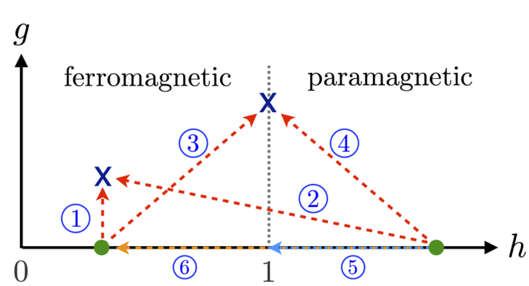

FIG. 1. Overview of the considered quench protocols in the transverse (h) vs longitudinal (g) field plane. Ground states are prepared in the ferromagnetic and paramagnetic phase of the purely transverse field Ising model (indicated by green dots) and quenched toward a nonintegrable semiclassical meson regime [types (1, 2)] and the integrable E_8 QFT regime (indicated by the gray dotted line) [types (3, 4)].

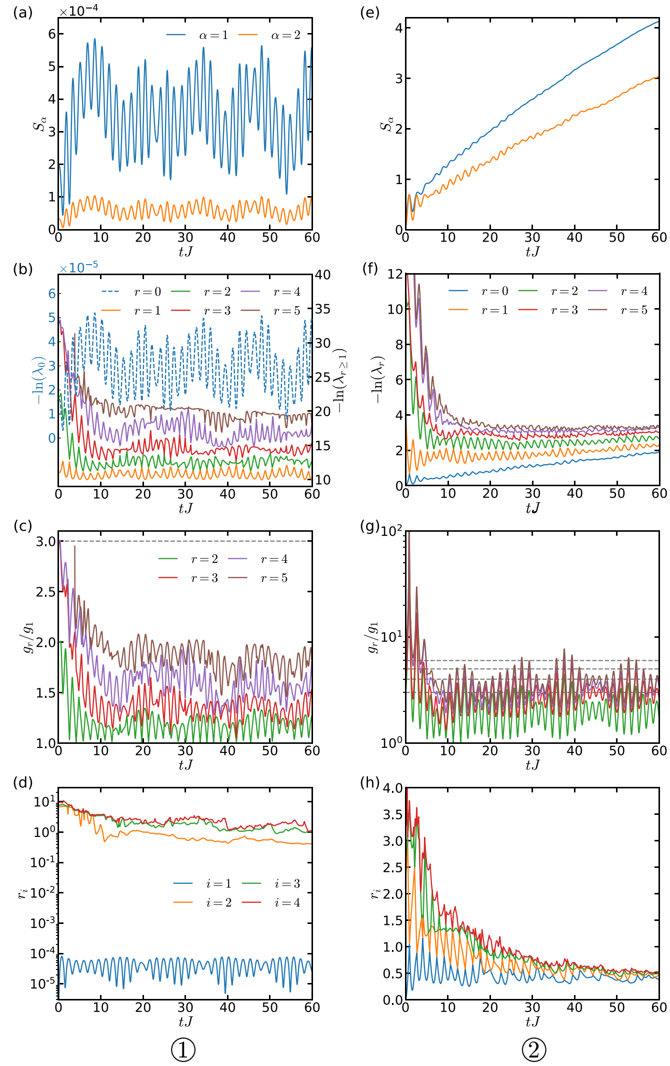

FIG. 2. Time dependence of physical quantities in quench protocols (1) [(a)–(d)] and (2) [(e)–(h)] to a semiclassical meson regime. From top to bottom: entanglement entropy S_1 and 2-Rényi entropy S_2 [(a), (e)], eigenvalues λ_r of the entanglement spectrum [(b), (f)], entanglement gap ratios $g_{r\geqslant 2}/g_1$ [(c), (g)], return rate functions r_i [(d), (h)]. See text for detailed discussion.

Majorana fermion QFT, given by the Hamiltonian [86]

$$H_{\rm IR} = \int_{-\infty}^{\infty} dx \left\{ \frac{i}{4\pi}(\psi\partial_x\psi - \bar{\psi}\partial_x\bar{\psi}) - \frac{iM_h}{2\pi}\bar{\psi}\psi + \mathcal{C}M_g^{15/8}\,\sigma \right\}. \qquad (3)$$

Here, $M_h \equiv 2J|1-h|$ is the free fermion mass, $M_g \equiv \mathcal{D}J\,|g|^{8/15}$ is a longitudinal mass scale, and $\mathcal{C} \approx 0.062$, $\mathcal{D} \approx 5.416$ are numerical constants [86,87]. The spin field σ is the continuous generalization of σ_j^z.

At criticality, i.e., for $M_h = M_g = 0$, the Hamiltonian (3) describes the Ising conformal field theory (CFT) of central charge $c = 1/2$, which possesses two scalar primary operators, $\epsilon = i\bar{\psi}\psi$ and σ with scaling dimensions $\Delta_\epsilon = 1$ and $\Delta_\sigma = 1/8$. Transverse perturbations of the Ising CFT ($M_h > 0, M_g = 0$) result in an integrable massive free fermion regime. Longitudinal perturbations confine domain walls as

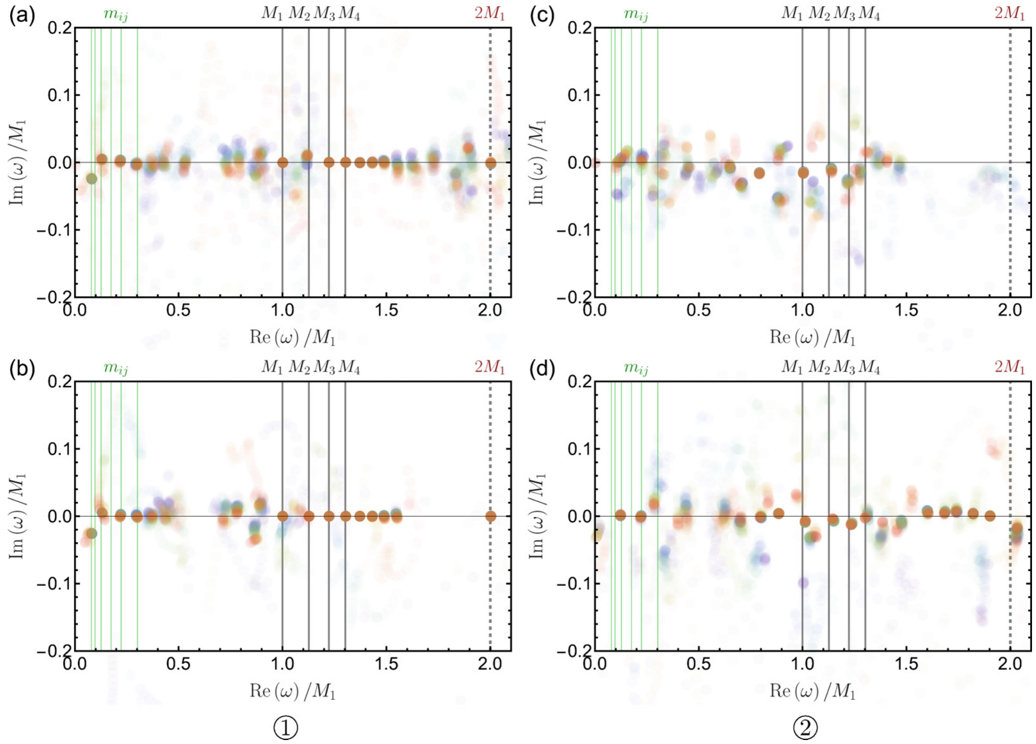

FIG. 3. Results of the Prony signal analysis of S_1 [(a), (c)] and $\xi_0 = -\ln(\lambda_0)$ [(b), (d)] under quench type (1) (left column) and (2) (right column). Gray vertical lines indicate meson masses M_i obtained from a semiclassical approximation; green vertical lines show all possible mass differences $m_{ij} \equiv |M_i - M_j|$ between them: m_{34}, m_{23}, m_{12}, m_{24}, m_{13}, m_{14} (ascending). The results demonstrate that the meson content of entanglement oscillations is fully encoded in the dominant eigenvalue of the modular Hamiltonian.

elementary excitations in the ferromagnetic phase into nonperturbative meson bound states [42]. In particular, pure longitudinal perturbations ($M_h = 0$, $M_g > 0$) give rise to the integrable and interacting E_8 QFT [88], whose 8 stable meson masses M_n are analytically known as ratios to the lightest mass $M_1 \equiv M_g$. Combined transverse and longitudinal perturbations ($M_h > 0, M_g > 0$) result in a nonintegrable interacting QFT with both stable and unstable mesonic bound states [89–92].

Setup. In the present Letter, we study real-time properties of entanglement spectra and return rate functions after global quantum quenches in both the integrable E_8 QFT as well as in the nonintegrable meson regime. For this purpose, we employ well established *ab initio* tensor network simulations, which directly give access to the quantities of interest in the thermodynamic limit of a translational invariant spin chain. In particular, based on the matrix product state (MPS) ansatz [93–96], we use the infinite time-evolving block decimation (iTEBD) algorithm [97] to construct a MPS approximation to (gapped) ground states $|\psi_0\rangle = \lim_{\beta\to\infty} e^{-\beta H_0}$ with respect to an Ising model Hamiltonian H_0 of the form (2) via imaginary-time evolution. We then use the same iTEBD algorithm to calculate its real-time evolution $|\psi(t)\rangle = e^{-itH_1}|\psi_0\rangle$ under a different Hamiltonian H_1. In nontrivial cases, the state $|\psi_0\rangle$ is not an eigenstate of H_1, such that this quench protocol drives the QMB system instantaneously out-of-equilibrium (at time $t = 0$) and causes the emergent phenomena.

We consider the specific quench protocols illustrated in Fig. 1. We choose two distinct prequench parameter points in the free fermion ferromagnetic and paramagnetic phase (shown as green dots) for the parameters $h = 0.25$ and $h = 1.75$, respectively. Protocols ① and ② quench toward a nonintegrable meson regime for which we exemplarily choose $\{h = 0.25, g = 0.1\}$ (indicated by the left cross). This quench point is far away from criticality; i.e., a QFT description is not amenable but instead a semiclassical approximation based on the Bohr-Sommerfeld quantization condition can be used to determine four meson states and their masses (see [45] for detailed discussions). Protocols ③ and ④, on the other hand, quench to the integrable E_8 QFT regime from the different prequench phases. The postquench parameter point is given for $\{h = 1, g = 0.48\}$ [98]. In Appendix A of the Supplemental Material [99] we contrast the resulting properties to a nonmesonic case, realized through quenches from the paramagnetic phase to the critical point (protocol ⑤; CFT results are available) and toward the ferromagnetic phase in the free fermion regime (protocol ⑥; regular DQPTs occur).

We analyze real-time entanglement properties of the state $|\psi(t)\rangle$ for a semi-infinite bipartition of the Ising chain, realized through a cut in between two repeating tensors of the translational invariant chain, which defines subsystem A as all the infinitely many sites to the left of the cut, and the complement B as all sites to the right. A Schmidt decomposition across this cut takes the form $|\psi(t)\rangle = \sum_r \sqrt{\lambda_r}\,|\psi_r^A\rangle \otimes |\psi_r^B\rangle$, where the Schmidt values $\lambda_0 \geqslant \lambda_1 \geqslant \lambda_2 \geqslant \dots$ are directly related to the eigenvalues ξ_r of the entanglement spectrum via $\lambda_r \equiv e^{-\xi_r}$. A relevant quantity of interest is the entanglement gaps $g_r \equiv \ln\lambda_0 - \ln\lambda_r = \xi_r - \xi_0$. The entanglement entropy is given by $S_1(\rho_A) = -\mathrm{Tr}_A[\rho_A \ln \rho_A] = -\sum_r \lambda_r \ln \lambda_r$ as the von Neumann entropy of the reduced density matrix,

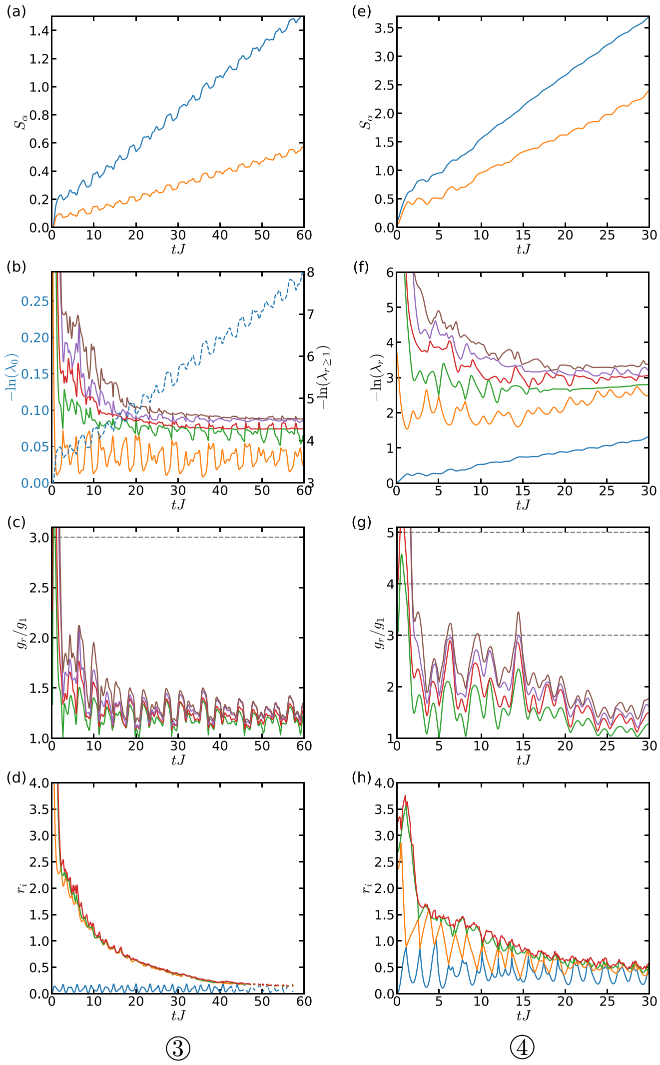

FIG. 4. Time dependence of physical quantities in quench protocols (3) [(a)–(d)] and (4) [(e)–(h)] to the integrable E_8 QFT regime. Legends and quantities are the same as in Fig. 2. See text for detailed discussion.

and the 2-Rényi entropy follows as $S_2(\rho_A) = -\ln \mathrm{Tr}_A \rho_A^2 = -\ln \sum_r \lambda_r^2$.

The central quantity to identify DQPTs is the Loschmidt amplitude $G(t) \equiv \langle\psi(0)|\psi(t)\rangle = \langle\psi(0)|e^{-itH_1}|\psi(0)\rangle$, from which the *return rate density* is defined as

$$r_1(t) = -\lim_{N\to\infty} \frac{1}{N} \ln |G(t)|^2. \tag{4}$$

The latter can be interpreted as an analog of the free energy density in equilibrium, such that nonanalyticities in $r_1(t)$ indicate the appearance of DQPTs as dynamical analogues of equilibrium phase transitions [50–52]. As discussed in [58], this definition can be generalized to the *rate functions*

$$r_i(t) = -2 \ln |\epsilon_i(t)|. \tag{5}$$

Here, ϵ_i are the eigenvalues (in decreasing order) of the mixed MPS transfer matrix $\mathcal{E}(t) \equiv \mathrm{Tr}_{\mathrm{phys}}[\bar{C}(0) \otimes C(t)]$ between two MPS tensors C of $|\psi_0\rangle$ and $|\psi(t)\rangle$, where a trace over physical indices is taken. Cusps or kinks in $r_1(t)$ correspond to level crossings between r_1 and $r_{i>1}$.

Quenches to nonintegrable semiclassical meson regimes. Figure 2 shows the simulation results for quenches from the ferromagnetic (type ①; left column) and paramagnetic phase (type ②; right column) into the nonintegrable semiclassical meson regime. The time evolution of S_1 and S_2 for quench ① [panel (a)] within the ferromagnetic phase exhibits a bounded oscillatory behavior, representing the known entanglement oscillations induced through meson confinement [45] [100]. On the other side, S_1 and S_2 show a very large entanglement growth under quench ② [panel (e)], which are superimposed with oscillations. The latter are, in contrast, unbounded in the available simulation times [101].

Panels (b) and (f) show the first eigenvalues $\xi_0, \ldots, \xi_5$ of the corresponding entanglement spectra. One can observe that the dominant eigenvalue $\xi_0 = -\ln(\lambda_0)$ in quench type ①, shown as the blue dashed curve in panel (b), oscillates on a much smaller magnitude (with respect to the left axis) than the remaining eigenvalues; i.e., the entanglement spectrum is largely gapped. The shape of ξ_0 follows nearly identically the time evolution of S_1 and hence seems to encode the entanglement oscillations (cf. the quantitative analyses below). In contrast, in all higher eigenvalues, many level crossings appear, indicated by nonanalyticities (cusps) of any single level. The same findings hold also for quench protocol ② [panel (f)] with the difference that ξ_0 is of the same scale as $\xi_{r\geqslant 1}$. Only at very early times after the quench, at $tJ \approx 0.9$, the entanglement spectrum becomes gapless, corresponding to a singularity in g_r/g_1 [cf. panel (g)].

The time dependence of the gap ratios g_r/g_1 is shown in panels (c) and (g) for $r = 2, \ldots, 5$. We want to contrast their behavior to CFT expectations in the case of quenches to the critical point (cf. Appendix A of the Supplemental Material). In the latter case, the ratios assume the constant values $g_r/g_1 = \Delta_r/\Delta_1$, where Δ_r are the conformal dimensions of primary fields and their descendants in the boundary CFT [30]. In the ferromagnetic meson quench in panel (c), all shown values are instead oscillating at later times around values smaller than the lowest integer CFT value $g_2/g_1 = 3$ (indicated by the gray dashed line). In particular, g_2/g_1 (green curve) exhibits multiple nonanalytic cusps, when the gap between ξ_1 and ξ_2 closes and the ratio hence assumes the value 1 as the lower bound. The same features exist also under quench ② [panel (g)]. Here, the oscillations display a larger amplitude and assume higher values (shown on a logarithmic scale), while a single singularity appears immediately after the quench [102]. Since also higher order ratios exhibit cusps, when the gap between other eigenvalues closes, these gap ratios do not contain information on meson masses.

The behavior of the first four return rate functions r_i is visible in panels (d) and (h). For quench protocol ①, r_1 is on a much smaller scale than all higher order ones. It exhibits regular oscillations, which carry the meson content of the postquench Hamiltonian (cf. the discussion below). On the other side, all r_i in quench type ② exhibit multiple level crossings. Since the first cusp in r_1 appears before the first minimum, we can identify them as *regular* ones according to the nomenclature in [55] [103]. In contrast to the DQPT regime in the transverse Ising model (cf. Fig. 6 in Appendix A

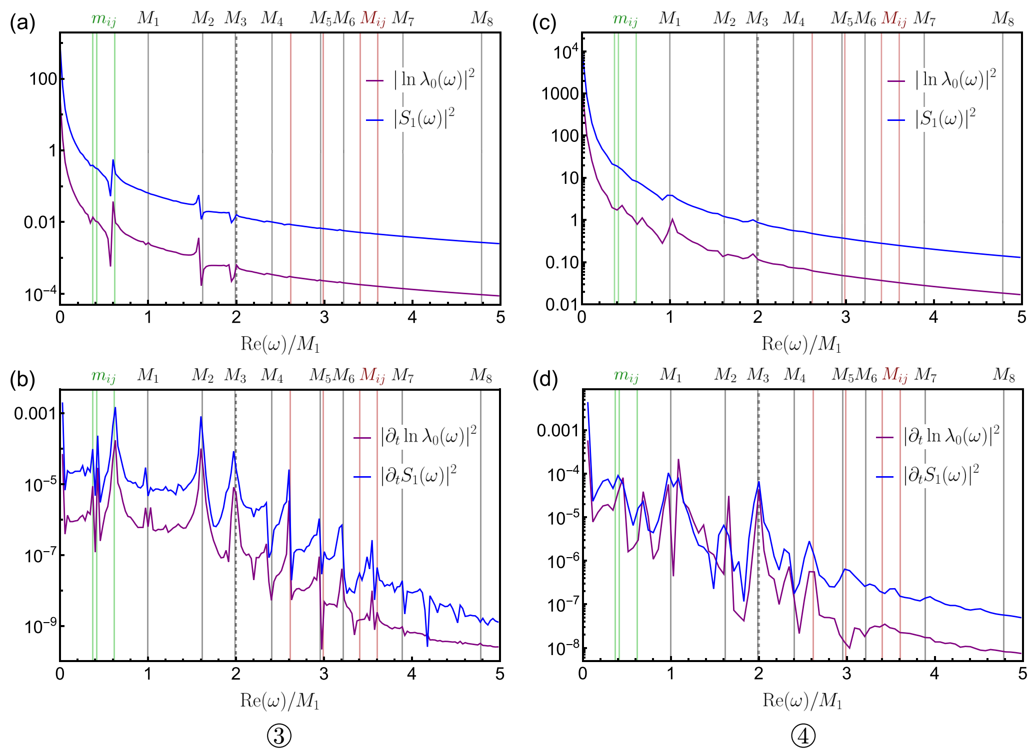

FIG. 5. Fourier spectra of ξ_0 and S_1 [(a), (c)], and their time derivatives [(b), (d)] under quench type (3) (left column) and (4) (right column). Green background lines mark the following mass differences: m_{23}, m_{34}, m_{12} (ascending). Red vertical lines indicate the following mass sums $M_{ij} \equiv M_i + M_j$: M_{12}, M_{13}, M_{14}, M_{23} (ascending). The results allow us to identify several meson states equally accurately from entanglement oscillations in S_1 and ξ_0.

of the Supplemental Material), which is also characterized by regular cusps, they are, however, not equally spaced in time. Moreover, while regular cusp positions coincide in the previous case with times when the entanglement spectrum becomes gapless [64], this is not a necessary consequence in the mesonic regime under consideration; i.e., the modular Hamiltonian remains gapped at these points in time, apart from the single exception at early times.

We use different methods in this Letter to analyze the meson content of entanglement spectra quantitatively and draw reliable interpretations from them. Figure 3 shows the results of a Prony signal analysis, whose basic idea is to represent a function as a sum of complex exponentials with frequencies plotted in the complex plane (see Appendix D for more details). The first row displays the analysis of S_1 in comparison to ξ_0 in the second row. In quench type ① [panels (a) and (b)] within the ferromagnetic phase, both quantities allow the clear and stable detection of four meson states M_i, which are consistent with a semiclassical approximation [45] (shown as gray vertical lines). Additionally, meson mass differences m_{ij} (shown as green vertical lines) and the continuum threshold at $2M_1$ can be identified. When the initial state is in the paramagnetic phase, i.e., for type ② [panels (c) and (d)], remnants of the meson states are still visible, but less clear due to the large entanglement growth. In both quenches, one can observe that ξ_0 even allows for a clearer extraction of meson poles in the Prony analyses than S_1. These analyses show that the meson content of the postquench Hamiltonian, giving rise to entanglement oscillations, is fully encoded in the dominant eigenvalue of the modular Hamiltonian [104]. Interestingly, r_1 in quench type ① equally encodes the meson masses in the frequency pattern, but in contrast to ξ_0, neither mass differences nor the continuum threshold are appearing.

Quenches to the integrable E_8 *QFT regime.* We now consider protocols ③ and ④, which quench toward the integrable E_8 QFT regime with 8 stable meson states. Figure 4 shows the simulation results. In type ③ [panel (a)], S_1 and S_2 show entanglement oscillations, which, in contrast to ①, are not bounded but superimposed with a linear growth. As discussed, e.g., in [105,106], such a behavior can be explained in a quasiparticle picture by mesons produced at finite velocity (due to a large quench magnitude), which are able to spread entanglement and quantum correlations faster. As in the previous section, the entanglement oscillations in the same quantities are much less pronounced under quench type ④ [panel (e)], when the initial state is in the paramagnetic phase.

The corresponding entanglement spectra [panels (b) and (f)] are gapped. As in the semiclassical regime, ξ_0 (blue curves) shares the qualitative behavior of S_1 in both quenches. Similarly, multiple level crossings appear in all higher order eigenvalues. The gap ratios g_r/g_1 [panels (c) and (g)] are oscillating around lower values than the constant CFT value. For g_2/g_1, the oscillations are broken by several cusps at the minimal lower value. While the return rate density r_1 in type ③ shows oscillations, which are given by the E_8 meson masses, only higher order rate functions $r_{i>1}$ exhibit level crossings [panel (d)] [107]. The same quantity in quench type ④ [panel (h)] instead has numerous regular cusps at unequally spaced positions, indicating the appearance of DQPTs.

Figure 5 shows a Fourier analysis of S_1 (blue curves) and ξ_0 (purple curves) for both quenches [panels (a) and (c)]. Due to the dominating linear entanglement growth, the Fourier spectra are decreasing toward larger frequencies and overall relatively flat with only small peak structures. For that reason we evaluate in panels (b) and (d) also their time derivatives, which allow us to identify the oscillating contributions more clearly. Several peaks become discernible that match the analytical E_8 meson mass ratios as well as some mass differences and sums. For quench ④ from the paramagnetic phase, these features are much less pronounced. There are only mild differences between the behavior of S_1 and ξ_0.

The discussions of this section exemplify that the previously found conclusions in the semiclassical meson regime hold equally also in the relativistic E_8 QFT. That is, the dominant eigenvalue of the entanglement spectrum fully encodes the meson content of the QMB system or QFT. The appearance of regular cusps at irregular positions, indicating the appearance of DQPTs, does not imply that the entanglement spectrum becomes gapless at these points in time.

Discussion and outlook. In this Letter we have studied the impact of meson confinement on the time evolution of the lowest eigenvalues in the entanglement spectrum and return rate functions after global quantum quenches in the Ising model. Our analyses contribute to a deeper understanding of entanglement properties of emergent phenomena in QMB systems and QFTs. The study of meson confinement and DQPT properties in the (1+1)-dimensional Ising QFT is a first step to more complex systems akin to QCD in particle physics. This necessarily involves the consideration of gauge theories, where the existence of DQPTs has been predicted in [108,109] and further investigated in [110,111]. Very recently, its first experimental observation was realized on a quantum computer and simultaneously discussed with entanglement tomography [112]. As a key implication of our study we see the potential use of such tomographic experiments to access the meson content of entanglement oscillations from the lowest part of the entanglement spectrum, instead of the experimentally inaccessible entanglement entropy itself.

Acknowledgments. We would like to thank Mari Carmen Bañuls, Jens Eisert, Jad C. Halimeh, Michal P. Heller, Jacopo Surace, and Luca Tagliacozzo for useful discussions and correspondence. J.K. is supported by the Israel Academy of Sciences and Humanities and the Council for Higher Education Excellence Fellowship Program for International Postdoctoral Researchers.

[1] E. Witten, APS medal for exceptional achievement in research: Invited article on entanglement properties of quantum field theory, Rev. Mod. Phys. **90**, 045003 (2018).

[2] B. Chen, B. Czech, and Z.-z. Wang, Quantum information in holographic duality, Rep. Prog. Phys. **85**, 046001 (2022).

[3] S. Catterall, R. Harnik, V. E. Hubeny, C. W. Bauer, A. Berlin, Z. Davoudi, T. Faulkner, T. Hartman, M. Headrick, Y. F. Kahn, *et al.*, Report of the Snowmass 2021 Theory Frontier Topical Group on Quantum Information Science, in *2022 Snowmass Summer Study*, https://inspirehep.net/conferences/1803127.

[4] M. Rangamani and T. Takayanagi, Holographic entanglement entropy, Lect. Notes Phys. **931**, 1 (2017).

[5] H. Li and F. D. M. Haldane, Entanglement Spectrum as a Generalization of Entanglement Entropy: Identification of Topological Order in Non-Abelian Fractional Quantum Hall Effect States, Phys. Rev. Lett. **101**, 010504 (2008).

[6] R. Haag, *Local Quantum Physics: Fields, Particles, Algebras* (Springer, Berlin, 1996).

[7] A. Chandran, M. Hermanns, N. Regnault, and B. A. Bernevig, Bulk-edge correspondence in entanglement spectra, Phys. Rev. B **84**, 205136 (2011).

[8] M. Dalmonte, V. Eisler, M. Falconi, and B. Vermersch, Entanglement Hamiltonians: From field theory, to lattice models and experiments, anna. der phys. **534**, 2200064 (2022).

[9] I. Peschel and V. Eisler, Reduced density matrices and entanglement entropy in free lattice models, J. Phys. A: Math. Theor. **42**, 504003 (2009).

[10] V. Alba, M. Haque, and A. M. Läuchli, Boundary-Locality and Perturbative Structure of Entanglement Spectra in Gapped Systems, Phys. Rev. Lett. **108**, 227201 (2012).

[11] V. Alba, M. Haque, and A. M. Läuchli, Entanglement Spectrum of the Two-Dimensional Bose-Hubbard Model, Phys. Rev. Lett. **110**, 260403 (2013).

[12] D. J. Luitz, N. Laflorencie, and F. Alet, Participation spectroscopy and entanglement Hamiltonian of quantum spin models, J. Stat. Mech. (2014) P08007.

[13] E. Tonni, J. Rodríguez-Laguna, and G. Sierra, Entanglement Hamiltonian and entanglement contour in inhomogeneous 1D critical systems, J. Stat. Mech. (2018) 043105.

[14] W. Zhu, Z. Huang, and Y.-C. He, Reconstructing entanglement Hamiltonian via entanglement eigenstates, Phys. Rev. B **99**, 235109 (2019).

[15] G. Giudici, T. Mendes-Santos, P. Calabrese, and M. Dalmonte, Entanglement Hamiltonians of lattice models via the Bisognano-Wichmann theorem, Phys. Rev. B **98**, 134403 (2018).

[16] G. Di Giulio, R. Arias, and E. Tonni, Entanglement Hamiltonians in 1D free lattice models after a global quantum quench, J. Stat. Mech. (2019) 123103.

[17] T. Mendes-Santos, G. Giudici, M. Dalmonte, and M. A. Rajabpour, Entanglement Hamiltonian of quantum critical chains and conformal field theories, Phys. Rev. B **100**, 155122 (2019).

[18] V. Eisler, G. Di Giulio, E. Tonni, and I. Peschel, Entanglement Hamiltonians for non-critical quantum chains, J. Stat. Mech. (2020) 103102.

[19] F. Rottoli, S. Scopa, and P. Calabrese, Entanglement Hamiltonian during a domain wall melting in the free Fermi chain, J. Stat. Mech. (2022) 063103.

[20] M. Song, J. Zhao, Z. Yan, and Z. Y. Meng, Reversing the Li and Haldane conjecture: The low-lying entanglement spectrum can also resemble the bulk energy spectrum, arXiv:2210.10062.

[21] V. Eisler and I. Peschel, Analytical results for the entanglement Hamiltonian of a free-fermion chain, J. Phys. A: Math. Theor. **50**, 284003 (2017).

[22] V. Eisler and I. Peschel, Properties of the entanglement Hamiltonian for finite free-fermion chains, J. Stat. Mech. (2018) 104001.

[23] F. Parisen Toldin and F. F. Assaad, Entanglement Hamiltonian of Interacting Fermionic Models, Phys. Rev. Lett. **121**, 200602 (2018).

[24] V. Eisler, E. Tonni, and I. Peschel, On the continuum limit of the entanglement Hamiltonian, J. Stat. Mech. (2019) 073101.

[25] P. Fries and I. A. Reyes, Entanglement Spectrum of Chiral Fermions on the Torus, Phys. Rev. Lett. **123**, 211603 (2019).

[26] J. J. Bisognano and E. H. Wichmann, On the duality condition for a Hermitian scalar field, J. Math. Phys. **16**, 985 (1975).

[27] J. J. Bisognano and E. H. Wichmann, On the duality condition for quantum fields, J. Math. Phys. **17**, 303 (1976).

[28] H. Casini, M. Huerta, and R. C. Myers, Towards a derivation of holographic entanglement entropy, J. High Energy Phys. 05 (2011) 036.

[29] X. Wen, S. Ryu, and A. W. W. Ludwig, Evolution operators in conformal field theories and conformal mappings: Entanglement Hamiltonian, the sine-square deformation, and others, Phys. Rev. B **93**, 235119 (2016).

[30] J. Cardy and E. Tonni, Entanglement Hamiltonians in two-dimensional conformal field theory, J. Stat. Mech. (2016) 123103.

[31] X. Wen, S. Ryu, and A. W. W. Ludwig, Entanglement Hamiltonian evolution during thermalization in conformal field theory, J. Stat. Mech. (2018) 113103.

[32] F. Pollmann and J. E. Moore, Entanglement spectra of critical and near-critical systems in one dimension, New J. Phys. **12**, 025006 (2010).

[33] J. I. Cirac, D. Poilblanc, N. Schuch, and F. Verstraete, Entanglement spectrum and boundary theories with projected entangled-pair states, Phys. Rev. B **83**, 245134 (2011).

[34] N. Schuch, D. Poilblanc, J. I. Cirac, and D. Pérez-García, Topological Order in the Projected Entangled-Pair States Formalism: Transfer Operator and Boundary Hamiltonians, Phys. Rev. Lett. **111**, 090501 (2013).

[35] T. H. Hsieh, L. Fu, and X.-L. Qi, Tensor network implementation of bulk entanglement spectrum, Phys. Rev. B **90**, 085137 (2014).

[36] L. Vanderstraeten, M. Mariën, J. Haegeman, N. Schuch, J. Vidal, and F. Verstraete, Bridging Perturbative Expansions with Tensor Networks, Phys. Rev. Lett. **119**, 070401 (2017).

[37] D. L. Jafferis and S. J. Suh, The gravity duals of modular Hamiltonians, J. High Energy Phys. 09 (2016) 068.

[38] D. L. Jafferis, A. Lewkowycz, J. Maldacena, and S. J. Suh, Relative entropy equals bulk relative entropy, J. High Energy Phys. 06 (2016) 004.

[39] W. Busza, K. Rajagopal, and W. van der Schee, Heavy ion collisions: The big picture, and the big questions, Annu. Rev. Nucl. Part. Sci. **68**, 339 (2018).

[40] A. Rothkopf, Heavy quarkonium in extreme conditions, Phys. Rep. **858**, 1 (2020).

[41] J. Berges, M. P. Heller, A. Mazeliauskas, and R. Venugopalan, QCD thermalization: *Ab initio* approaches and interdisciplinary connections, Rev. Mod. Phys. **93**, 035003 (2021).

[42] B. M. McCoy and T. T. Wu, Two-dimensional Ising field theory in a magnetic field: Breakup of the cut in the two point function, Phys. Rev. D **18**, 1259 (1978).

[43] F. Liu, R. Lundgren, P. Titum, G. Pagano, J. Zhang, C. Monroe, and A. V. Gorshkov, Confined Quasiparticle Dynamics in Long-Range Interacting Quantum Spin Chains, Phys. Rev. Lett. **122**, 150601 (2019).

[44] A. Lerose, B. Zunkovic, A. Silva, and A. Gambassi, Quasilocalized excitations induced by long-range interactions in translationally invariant quantum spin chains, Phys. Rev. B **99**, 121112(R) (2019).

[45] M. Kormos, M. Collura, G. Takacs, and P. Calabrese, Real-time confinement following a quantum quench to a non-integrable model, Nat. Phys. **13**, 246 (2017).

[46] J. Surace, L. Tagliacozzo, and E. Tonni, Operator content of entanglement spectra in the transverse field Ising chain after global quenches, Phys. Rev. B **101**, 241107(R) (2020).

[47] N. F. Robertson, J. Surace, and L. Tagliacozzo, Quenches to the critical point of the three-state Potts model: Matrix product state simulations and conformal field theory, Phys. Rev. B **105**, 195103 (2022).

[48] K. Okunishi, T. Nishino, and H. Ueda, Developments in the tensor network—from statistical mechanics to quantum entanglement, J. Phys. Soc. Jpn. **91**, 062001 (2022).

[49] M. C. Bañuls, Tensor network algorithms: A route map, arXiv:2205.10345.

[50] M. Heyl, Dynamical quantum phase transitions: A review, Rep. Prog. Phys. **81**, 054001 (2018).

[51] M. Heyl, Dynamical quantum phase transitions: A brief survey, Europhys. Lett. **125**, 26001 (2019).

[52] M. Heyl, A. Polkovnikov, and S. Kehrein, Dynamical Quantum Phase Transitions in the Transverse-Field Ising Model, Phys. Rev. Lett. **110**, 135704 (2013).

[53] C. Karrasch and D. Schuricht, Dynamical phase transitions after quenches in nonintegrable models, Phys. Rev. B **87**, 195104 (2013).

[54] B. Žunkovič, M. Heyl, M. Knap, and A. Silva, Dynamical Quantum Phase Transitions in Spin Chains with Long-Range Interactions: Merging Different Concepts of Nonequilibrium Criticality, Phys. Rev. Lett. **120**, 130601 (2018).

[55] J. C. Halimeh and V. Zauner-Stauber, Dynamical phase diagram of quantum spin chains with long-range interactions, Phys. Rev. B **96**, 134427 (2017).

[56] P. Jurcevic, H. Shen, P. Hauke, C. Maier, T. Brydges, C. Hempel, B. P. Lanyon, M. Heyl, R. Blatt, and C. F. Roos, Direct Observation of Dynamical Quantum Phase Transitions in an Interacting Many-Body System, Phys. Rev. Lett. **119**, 080501 (2017).

[57] J. Zhang, G. Pagano, P. W. Hess, A. Kyprianidis, P. Becker, H. Kaplan, A. V. Gorshkov, Z. X. Gong, and C. Monroe, Observation of a many-body dynamical phase transition with a 53-qubit quantum simulator, Nature (London) **551**, 601 (2017).

[58] V. Zauner-Stauber and J. C. Halimeh, Probing the anomalous dynamical phase in long-range quantum spin chains through Fisher-zero lines, Phys. Rev. E **96**, 062118 (2017).

[59] J. C. Halimeh, M. Van Damme, V. Zauner-Stauber, and L. Vanderstraeten, Quasiparticle origin of dynamical quantum phase transitions, Phys. Rev. Res. **2**, 033111 (2020).

[60] T. Hashizume, I. P. McCulloch, and J. C. Halimeh, Dynamical phase transitions in the two-dimensional transverse-field Ising model, Phys. Rev. Res. **4**, 013250 (2022).

[61] N. Defenu, T. Enss, and J. C. Halimeh, Dynamical criticality and domain-wall coupling in long-range Hamiltonians, Phys. Rev. B **100**, 014434 (2019).
[62] J. C. Halimeh, M. Van Damme, L. Guo, J. Lang, and P. Hauke, Dynamical phase transitions in quantum spin models with antiferromagnetic long-range interactions, Phys. Rev. B **104**, 115133 (2021).
[63] E. Canovi, E. Ercolessi, P. Naldesi, L. Taddia, and D. Vodola, Dynamics of entanglement entropy and entanglement spectrum crossing a quantum phase transition, Phys. Rev. B **89**, 104303 (2014).
[64] G. Torlai, L. Tagliacozzo, and G. D. Chiara, Dynamics of the entanglement spectrum in spin chains, J. Stat. Mech. (2014) P06001.
[65] S. De Nicola, A. A. Michailidis, and M. Serbyn, Entanglement View of Dynamical Quantum Phase Transitions, Phys. Rev. Lett. **126**, 040602 (2021).
[66] R. Jafari and A. Akbari, Floquet dynamical phase transition and entanglement spectrum, Phys. Rev. A **103**, 012204 (2021).
[67] Y. Alexeev, D. Bacon, K. R. Brown, R. Calderbank, L. D. Carr, F. T. Chong, B. DeMarco, D. Englund, E. Farhi, B. Fefferman *et al.*, Quantum Computer Systems for Scientific Discovery, PRX Quantum **2**, 017001 (2021).
[68] C. W. Bauer, Z. Davoudi, A. B. Balantekin, T. Bhattacharya, M. Carena, W. A. de Jong, P. Draper, A. El-Khadra, N. Gemelke, M. Hanada *et al.*, Quantum simulation for high energy physics, arXiv:2204.03381.
[69] J. Fraxanet, T. Salamon, and M. Lewenstein, The coming decades of quantum simulation, arXiv:2204.08905.
[70] A. J. Daley, I. Bloch, C. Kokail, S. Flannigan, N. Pearson, M. Troyer, and P. Zoller, Practical quantum advantage in quantum simulation, Nature (London) **607**, 667 (2022).
[71] W. L. Tan, P. Becker, F. Liu, G. Pagano, K. S. Collins, A. De, L. Feng, H. B. Kaplan, A. Kyprianidis, R. Lundgren *et al.*, Domain-wall confinement and dynamics in a quantum simulator, Nat. Phys. **17**, 742 (2021).
[72] J. Mildenberger, W. Mruczkiewicz, J. C. Halimeh, Z. Jiang, and P. Hauke, Probing confinement in a $\mathbb{Z}_2$ lattice gauge theory on a quantum computer, arXiv:2203.08905.
[73] R. Verdel, F. Liu, S. Whitsitt, A. V. Gorshkov, and M. Heyl, Real-time dynamics of string breaking in quantum spin chains, Phys. Rev. B **102**, 014308 (2020).
[74] F. M. Surace and A. Lerose, Scattering of mesons in quantum simulators, New J. Phys. **23**, 062001 (2021).
[75] P. I. Karpov, G. Y. Zhu, M. P. Heller, and M. Heyl, Spatiotemporal dynamics of particle collisions in quantum spin chains, Phys. Rev. Res. **4**, L032001 (2022).
[76] M. Rigobello, S. Notarnicola, G. Magnifico, and S. Montangero, Entanglement generation in (1+1)D QED scattering processes, Phys. Rev. D **104**, 114501 (2021).
[77] J. Knaute and P. Hauke, Relativistic meson spectra on ion-trap quantum simulators, Phys. Rev. A **105**, 022616 (2022).
[78] J. C. Halimeh, I. P. McCulloch, B. Yang, and P. Hauke, Tuning the topological θ-angle in cold-atom quantum simulators of gauge theories, PRX Quantum **3**, 040316 (2022).
[79] M. C. Banuls, M. P. Heller, K. Jansen, J. Knaute, and V. Svensson, A quantum information perspective on meson melting, arXiv:2206.10528.
[80] M. Kebrič, U. Borla, U. Schollwöck, S. Moroz, L. Barbiero, and F. Grusdt, Confinement induced frustration in a one-dimensional $\mathbb{Z}_2$ lattice gauge theory, New J. Phys. **25**, 013035 (2023).
[81] M. A. Werner, C. P. Moca, M. Kormos, O. Legeza, B. Dóra, and G. Zaránd, Spectroscopic evidence for engineered hadron formation in repulsive fermionic SU(N) Hubbard models, arXiv:2207.00994.
[82] M. Dalmonte, B. Vermersch, and P. Zoller, Quantum simulation and spectroscopy of entanglement Hamiltonians, Nat. Phys. **14**, 827 (2018).
[83] C. Kokail, R. van Bijnen, A. Elben, B. Vermersch, and P. Zoller, Entanglement Hamiltonian tomography in quantum simulation, Nat. Phys. **17**, 936 (2021).
[84] C. Kokail, B. Sundar, T. V. Zache, A. Elben, B. Vermersch, M. Dalmonte, R. van Bijnen, and P. Zoller, Quantum Variational Learning of the Entanglement Hamiltonian, Phys. Rev. Lett. **127**, 170501 (2021).
[85] S. Sachdev, *Quantum Phase Transitions*, 2nd ed. (Cambridge University Press, Cambridge, UK, 2011).
[86] T. Rakovszky, M. Mestyán, M. Collura, M. Kormos, and G. Takács, Hamiltonian truncation approach to quenches in the Ising field theory, Nucl. Phys. B **911**, 805 (2016).
[87] K. Hódsági, M. Kormos, and G. Takács, Quench dynamics of the Ising field theory in a magnetic field, SciPost Phys. **5**, 027 (2018).
[88] A. B. Zamolodchikov, Integrals of motion and S-matrix of the (scaled) $T = T_c$ Ising model with magnetic field, Int. J. Mod. Phys. A **04**, 4235 (1989).
[89] G. Delfino, G. Mussardo, and P. Simonetti, Nonintegrable quantum field theories as perturbations of certain integrable models, Nucl. Phys. B **473**, 469 (1996).
[90] G. Delfino, P. Grinza, and G. Mussardo, Decay of particles above threshold in the Ising field theory with magnetic field, Nucl. Phys. B **737**, 291 (2006).
[91] P. Fonseca and A. Zamolodchikov, Ising spectroscopy. I. Mesons at $T < T_c$, arXiv:hep-th/0612304.
[92] A. Zamolodchikov, Ising spectroscopy. II. Particles and poles at $T > T_c$, arXiv:1310.4821.
[93] F. Verstraete, V. Murg, and J. Cirac, Matrix product states, projected entangled pair states, and variational renormalization group methods for quantum spin systems, Adv. Phys. **57**, 143 (2008).
[94] U. Schollwöck, The density-matrix renormalization group in the age of matrix product states, Ann. Phys. **326**, 96 (2011).
[95] J. I. Cirac and F. Verstraete, Renormalization and tensor product states in spin chains and lattices, J. Phys. A: Math. Theor. **42**, 504004 (2009).
[96] R. Orus, A practical introduction to tensor networks: Matrix product states and projected entangled pair states, Ann. Phys. **349**, 117 (2014).
[97] G. Vidal, Classical Simulation of Infinite-Size Quantum Lattice Systems in One Spatial Dimension, Phys. Rev. Lett. **98**, 070201 (2007).
[98] The values are chosen such that both final quench points have an identical mass gap, given by the first meson mass $M_1/J \approx 3.66$.
[99] See Supplemental Material at http://link.aps.org/supplemental/10.1103/PhysRevB.107.L100303 (including Refs. [30,46,113–115]) for several appendices containing further background material.

[100] We have chosen the parameters in quench protocol ① identical to one of the cases in [45] and hence reproduce the form of S_1 here.
[101] We refer to Appendix B of the Supplemental Material for some details of the iTEBD simulations.
[102] We refer to Appendix C of the Supplemental Material for a comparison of the ratio g_2/g_1 in all quench examples.
[103] While we do not observe any nonanalyticities in quench type ①, the existence of *anomalous* cusps [55] could be possible for other quench parameters within the ferromagnetic phase.
[104] All higher order eigenvalues and gaps exhibit nonanalytic cusps in their profile and hence do not allow us to define oscillation frequencies, which could be quantitatively analyzed.
[105] S. Birnkammer, A. Bastianello, and M. Knap, Prethermalization in confined spin chains, Nat. Comm. **13**, 7663 (2022).
[106] S. Scopa, P. Calabrese, and A. Bastianello, Entanglement dynamics in confining spin chains, Phys. Rev. B **105**, 125413 (2022).
[107] In the calculation of r_i, some numerical exception errors occur at late times. The corresponding data points are left blank in panel (d).
[108] Y.-P. Huang, D. Banerjee, and M. Heyl, Dynamical Quantum Phase Transitions in U(1) Quantum Link Models, Phys. Rev. Lett. **122**, 250401 (2019).
[109] T. V. Zache, N. Mueller, J. T. Schneider, F. Jendrzejewski, J. Berges, and P. Hauke, Dynamical Topological Transitions in the Massive Schwinger Model with a θ Term, Phys. Rev. Lett. **122**, 050403 (2019).
[110] M. Van Damme, T. V. Zache, D. Banerjee, P. Hauke, and J. C. Halimeh, Dynamical quantum phase transitions in spin-SU(1) quantum link models, Phys. Rev. B **106**, 245110 (2022).
[111] M. Van Damme, J.-Y. Desaules, Z. Papić, and J. C. Halimeh, The anatomy of dynamical quantum phase transitions, arXiv:2210.02453.
[112] N. Mueller, J. A. Carolan, A. Connelly, Z. Davoudi, E. F. Dumitrescu, and K. Yeter-Aydeniz, Quantum computation of dynamical quantum phase transitions and entanglement tomography in a lattice gauge theory, arXiv:2210.03089.
[113] P. Calabrese and J. L. Cardy, Evolution of entanglement entropy in one-dimensional systems, J. Stat. Mech. (2005) P04010.
[114] T. Peter, Generalized Prony method, Ph.D. thesis, University of Göttingen, 2014, http://na.math.uni-goettingen.de/pdf/Pe13.pdf.
[115] M. C. Banuls, M. P. Heller, K. Jansen, J. Knaute, and V. Svensson, From spin chains to real-time thermal field theory using tensor networks, Phys. Rev. Res. **2**, 033301 (2020).